Supporting Information for "Some lava flows may not have been as thick as they appear"

Jonas Katona[1,2], Xiaojing Fu[1,3], Tushar Mittal[1,4], Michael Manga[1], and Stephen Self[1].

[1]University of California Berkeley, Berkeley, CA, United States

[2]Yale University, New Haven, CT, United States

[3]California Institute of Technology, Pasadena, CA, United States

[4]Massachusetts Institute of Technology, Cambridge, MA, United States

Contents of this file

Texts S1 to S3

Figures S1 to S7

Additional Supporting Information (Files uploaded separately)

Captions for Movies S1 to S3

Introduction

In Text S1, we describe how we derived or calibrated the phase-field parameters τ, ω_ϕ^2, and H from either known quantities or the interface width d, which numerically acts somewhat like a viscosity/smoothing term. Figure S1 also gives relevant details as to how

we calibrated d. In Text S2, we define and explain the relative L^2 error, which is used in Figure S2. In Text S3, we describe the choice of grid size Δx for each simulation. Figures S2-S7 describe and showcase several compelling yet somewhat tangential properties we observed in our simulations, as well as detailed descriptions about how qualitative aspects of the lava solidification dynamics change with the emplacement time interval t_{emp} and lobe height h. Finally, we provide captions for three movies which correspond to the three cases featured in Figure 1.

Text S1. Formulation of parameters

Rewriting the parameters in (Kim & Kim, 2005) in terms of the parameters in our model, we have that $\omega = H$, $M_\phi = M$, $\varepsilon = \varepsilon_\phi$, $D_T = \alpha$, $\Delta H_m = L$, $g(\phi) = \phi^2(1-\phi)^2$, $f_c = 0$, and $f_\phi(\phi, T) = \frac{(T-T_m)L}{T_m} P'(\phi)$, where $P(\phi) = (3-2\phi)\phi^2$. Then, from here, we go through the same derivations in (Kim & Kim, 2005) to derive the interface width $d = 2\xi$ and the interface energy σ.

Consider a partially-solidified lava system at equilibrium where we have a 1D interface between solid $\phi = 1$ at $x = d$ and liquid $\phi = 0$ at $x = 0$. Since this system is at equilibrium and we assume the equal temperature condition for pure substances, $\partial_t \phi = \partial_t T = 0$ and $T = T_m$, such that equation (1) from the main paper (the PDE for the phase, ϕ) can be integrated for the equilibrium phase-field profile $\phi_0(x)$.

$$\begin{aligned} &\omega_\phi^2 \partial_x^2 \phi_0 - g'(\phi_0) - \frac{L}{H}\frac{(T_m - T_m)}{T_m} P'(\phi_0) = 0 \Rightarrow \omega_\phi^2 \partial_x \phi_0 \partial_x^2 \phi_0 - \partial_x \phi_0 g'(\phi_0) = 0 \\ &\Rightarrow \frac{d}{dx}\left[\frac{1}{2}\omega_\phi^2 (\partial_x \phi_0)^2 - g(\phi_0)\right] = 0 \Rightarrow \frac{1}{2}\omega_\phi^2 (\partial_x \phi_0)^2 - g(\phi_0) = \text{const.}, \end{aligned} \tag{1}$$

where we assume that ω_ϕ is a constant and const. $= \frac{1}{2}\omega_\phi^2 (\partial_x \phi_0(x_0))^2 - g(\phi_0(x_0))$ at some reference position x_0. Finally, without loss of generality, we can let $x_0 = 0$ and put a

Dirichlet boundary condition here (we would expect one anyways if the lava is fully liquid there), such that $g\left(\phi_0\left(x_0\right)\right) = g\left(\phi_0\left(0\right)\right) = g\left(0\right) = 0$ and $\partial_x\phi_0\left(x_0\right) = \partial_x\phi_0\left(0\right) = 0$. Hence, const. $= 0$ in (1), in which case we can integrate (1):

$$\frac{1}{2}\omega_\phi^2\left(\partial_x\phi_0\right)^2 = g\left(\phi_0\right) \Rightarrow \frac{\partial\phi_0}{\partial x} = \sqrt{\frac{2}{\omega_\phi^2}g\left(\phi_0\right)}$$
$$\Rightarrow d = \int_{\phi_a}^{\phi_b}\frac{d\phi_0}{\sqrt{\frac{2}{\omega_\phi^2}g\left(\phi_0\right)}} = \frac{\omega_\phi}{\sqrt{2}}\int_{\phi_a}^{\phi_b}\frac{d\phi_0}{\left|\phi_0\right|\left|1-\phi_0\right|}. \tag{2}$$

As in Kim and Kim, we use $\phi_a = 0.1$ and $\phi_b = 0.9$ to integrate (2), from which we get that

$$d = \omega_\phi 2\sqrt{2}\ln 3, \tag{3}$$

which is essentially the same result derived in (Kim & Kim, 2005).

Next, to obtain the interface energy, we again repeat the steps in (Kim & Kim, 2005) by considering an equilibrium system with a cylindrical solid in liquid matrix while maintaining a diffuse interface between them. This gives us the following:

$$\sigma = \varepsilon_\phi^2\int_{-\infty}^{\infty}\left(\frac{d\phi_0}{dr}\right)^2 dr = \sqrt{2}\varepsilon_\phi\int_0^1\sqrt{Hg\left(\phi_0\right)}d\phi_0$$
$$= \sqrt{2}\varepsilon_\phi\sqrt{H}\int_0^1\left|\phi_0\right|\left|1-\phi_0\right|d\phi_0 = \frac{\varepsilon_\phi}{3}\sqrt{\frac{H}{2}}. \tag{4}$$

Making necessary assumptions in the thin interface limit, equation (22) from (Kim & Kim, 2005) gives us that

$$J = \int_0^1\frac{h_p\left(\phi\right)\left[1-h_d\left(\phi\right)\right]}{\sqrt{g\left(\phi\right)}}d\phi$$
$$= \int_0^1\frac{\phi^3\left(6\phi^2-15\phi+10\right)\left[1-\phi^3\left(6\phi^2-15\phi+10\right)\right]}{\left|\phi\right|\left|1-\phi\right|}d\phi = \frac{209}{420}. \tag{5}$$

Thus, using (5), equation (21) in Kim and Kim implies that

$$\beta = \frac{1}{3\sqrt{2}}\frac{T_m\sqrt{H}}{\varepsilon_\phi LM} - \frac{L}{\alpha c_p}\frac{\varepsilon_\phi}{\sqrt{2H}}J = \frac{1}{3\sqrt{2}}\frac{T_m\sqrt{H}}{\varepsilon_\phi LM} - \frac{209}{420}\frac{L}{\alpha c_p}\frac{\varepsilon_\phi}{\sqrt{2H}}. \tag{6}$$

Our only unknown parameter is $\omega_\phi \sim d$, which we have to adjust as we run simulations to match known solidification data, but once given ω_ϕ and d, we can derive H, τ, and ε_ϕ. Therefore, our parameter search is only *one-dimensional*, since once we choose a value of d or ω_ϕ, all other parameters can be immediately determined.

Using equations $\omega_\phi = \varepsilon_\phi/\sqrt{H}$ and $\tau = 1/(HM)$ from (Provatas & Elder, 2010) along with (3), (4), and (6) above, we can rewrite all unmeasured parameters in terms of measurable quantities and d as follows:

$$\omega_\phi = \frac{\sqrt{2}}{4\ln 3}d, \quad H = 12\ln 3\frac{\sigma}{d}, \quad \tau = \frac{1}{8\ln^2 3}\frac{d^2 L}{\sigma T_m}\left(\beta + \frac{209}{1680\ln 3}\frac{dL}{\alpha c_p}\right). \tag{7}$$

Using the sample parameters from Table 1 in the main paper, the last two equations in (7) become

$$H \approx \frac{6.592}{d}\ \text{J m}^{-2}, \quad \tau \approx 2.899\times 10^6 d^3\ \text{s m}^{-3} + 3.454\times 10^{-6} d^2\ \text{s m}^{-2}. \tag{8}$$

Even if the solid-liquid interface width were microscopic, i.e., $d \sim 10^{-9}$ m, the second equation in (8) would still imply that $3.454\times 10^{-6} d^2\ \text{s m}^{-2} \ll 2.899\times 10^6 d^3\ \text{s m}^{-3}$, since in that case, $\frac{3.454\times 10^{-6} d^2\ \text{s m}^{-2}}{2.899\times 10^6 d^3\ \text{s m}^{-3}} \sim 10^{-3}$. Thus, we can further make the simplification $\tau \approx 2.899\times 10^6 d^3\ \text{s m}^{-3}$, and in general, for parameters similar to basalt lava, the third equation in (7) can be simplified to

$$\tau = \frac{209}{13440\ln^3 3}\frac{d^3 L^2}{\alpha c_p \sigma T_m}. \tag{9}$$

Finally, by the above considerations and equations, we can also derive the following informative scaling properties:

$$\omega_\phi \sim d, \quad H \sim \frac{\sigma}{d}, \quad \tau \sim \frac{d^3 L^2}{\alpha c_p \sigma T_m}, \quad M \sim \frac{\alpha c_p T_m}{d^2 L^2}, \quad \varepsilon_\phi \sim \sqrt{\sigma}\sqrt{d}. \tag{10}$$

The scaling relationships in (10) provide a physical interpretation of these variables, as well as simple sanity-checks of the validity of the assumptions we made for a given choice of parameters. And as mentioned in (Kim & Kim, 2005), (10) should in theory hold as long as $d \ll \alpha/V$ and $d \ll R$, where V and R are the velocity of the solidification front and the local radius of curvature for the solid-liquid interface, respectively.

Text S2. Definition of relative $\mathbf{L}^2$ error

Say we have n data points in space. Suppose that $f(x)$ is our exact function and $\widehat{f}(x)$ is an approximation for f. Then, the exact L^2 error on $[0, L]$ would be

$$e = \left[\int_0^L \left(f(x) - \widehat{f}(x)\right)^2 dx\right]^{1/2}.$$

However, given that $\widehat{f}$ lives on a grid with n points and spatial intervals of size Δx, we have to approximate e as follows, using a Riemann sum:

$$e \approx \left[\Delta x \sum_{i=1}^{n} \left(f(x_i) - \widehat{f}(x_i)\right)^2\right]^{1/2},$$

where $x_n = L$ and $x_1 = \Delta x$. Finally, to compute the relative L^2 error, e_{rel}, we divide e by the L^2 norm of f, i.e.,

$$e_{\text{rel}} \approx \frac{\left[\Delta x \sum_{i=1}^{n} \left(f(x_i) - \widehat{f}(x_i)\right)^2\right]^{1/2}}{\left[\Delta x \sum_{i=1}^{n} f(x_i)^2\right]^{1/2}} = \left[\frac{\sum_{i=1}^{n} \left(f(x_i) - \widehat{f}(x_i)\right)^2}{\sum_{i=1}^{n} f(x_i)^2}\right]^{1/2}.$$

Text S3. Spatial grid size Δx

The spatial grid size we use is

$$\Delta x = 10^{-3} \min \left\{ \text{nint} \left(\sqrt{10h} \right), 10 \right\}, \tag{11}$$

where nint is the function which rounds its argument to the nearest integer. Intuitively, we can think of Equation 11 as interpolating Δx from 10^{-3} (for $h = 0.1, 0.2$) to 10^{-2} (for $h = 10, 15, 20$) using the square root function, except rounding each value to the third decimal place for simplicity's sake. That way, Δx roughly scales with h, which balances computational efficiency with numerical precision.

Figure S2 Caption. Using nonlinear least squares, we fit the solidification data for a *single* lobe cooling by itself to the function

$$t_h = \frac{h^2}{\alpha} \left[\frac{A}{h^B} + C \exp\left(-Dh\right) + E \right] \tag{12}$$

which heuristically models the nonlinear trend after the conventional cooling estimate $t_h \sim h^2$ derived from solving the Stefan problem. The best fit parameters we find are $A \approx 0.0110$, $B \approx 0.2294$, $C \approx 0.3346$, $D \approx 24.8922$, and $E \approx 0.0320$. With these parameters, the relative L^2 error (as defined in Text S2) between $t_h \alpha / h^2$ as fitted above and the actual data is $\approx 9.8237 \times 10^{-3} < 1\%$, which shows very respectable agreement. Hence, (12) could be a starting point for modeling t_h with more general physical parameters and initial conditions.

By using the term "strong nonlinearity" in Figure S2, we are referring to how there is a qualitative difference in the curve for small enough lobe sizes. This difference is best explained by the quick decay of the exponential term in our curve fit: For h not too large, the exponential term quickly disappears and the trend becomes primarily dominated by

the power law term. Hence, motivated by how the relative L^2 error between our best-fit curve and numerical solution is just under 1%, we heuristically have drawn the line between the "strongly nonlinear" and "weakly nonlinear" regions by indicating where the relative error between the fit with and without the exponential term falls below 1%. That point is at roughly $h = 0.26344$, after which the exponential term contributes an error which is below 1% and decreases further as h increases.

We label these two regions in Figure S2 to give a rough estimate of where the usual $t_h \sim h^2$ scaling relationships are relatively valid, and show how for small enough lobe sizes, deviations from this trend begin to dominate significantly. The physical interpretation of these regions is as follows: As we work with smaller and smaller lobes, the nonlinear effects of convection cooling and radiative heat loss at the lava surface begin to dominate the time it takes for a lobe of that size to cool. The usual Stefan problem formulation often ignores these nonlinear effects in the boundary condition at the lava-air interface, but based off of our results here, we suggest that these will contribute a non-negligible effect to the solution when the lobe size is too small.

Notes for Figures S3-S7. For Figures S3-S7, we will consider the trends between different lobe thicknesses once we weight the emplacement time by t_h. For every dimensionless plot, the stars (*) represent merged cases, the crosses ($\times$) represent in parallel cases, and the pluses (+) represent in sequence cases.

Movie S1. Under the folder `movies` in the GitHub data repository, `emplacementresults_10_10_843K_406` is a movie showing the solidification dynamics for the fused flow case shown in Figure 1.

Movie S2. Under the folder `movies`, `emplacementresults_10_10_843K_3250hours.mp4` is a movie showing the solidification dynamics for the in parallel case shown in Figure 1.

Movie S3. Under the folder `movies`, `emplacementresults_10_10_843K_26000hours.mp4` is a movie showing the solidification dynamics for the in sequence case shown in Figure 1.

References

Kim, S. G., & Kim, W. T. (2005). Phase-Field Modeling of Solidification. In *Handbook of materials modeling* (pp. 2105–2116). Springer, Dordrecht.

Provatas, N., & Elder, K. (2010). *Phase-field methods in materials science and engineering* (1st ed.). Wiley.

Wright, T. L., & Marsh, B. (2016). Quantification of the intrusion process at Kīlauea volcano, Hawai'i. *Journal of Volcanology and Geothermal Research*, *328*, 34–44.

Wright, T. L., & Okamura, R. T. (1977). *Cooling and crystallization of tholeiitic basalt, 1965 Makaopuhi Lava Lake, Hawaii* (Tech. Rep.).

Wright, T. L., Peck, D. L., & Shaw, H. R. (1972). *Kilauea Lava Lakes: Natural Laboratories for Study of Cooling, Crystallization, and Differentiation of Basaltic Magma* (Vol. 19).

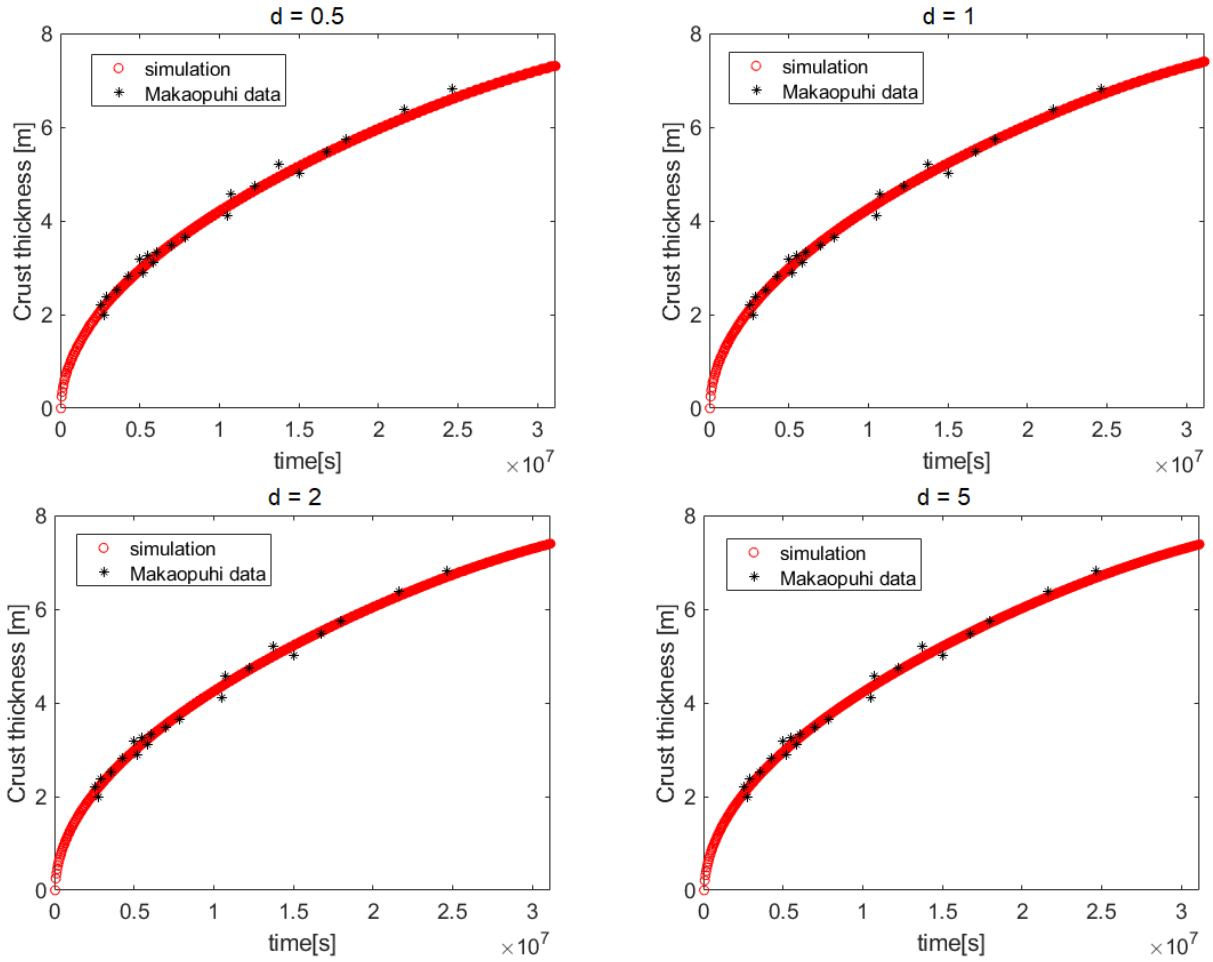

Figure S1. The open red circles track how our simulated solidified crust thickness vs. time varies with the interface width d, while the stars mark known field data measured from Makaopuhi lava lake (Wright & Okamura, 1977; Wright et al., 1972; Wright & Marsh, 2016). All other physical parameters that we used are given in Table 1, with initial conditions consisting of a lava lake of arbitrarily large depth and initial temperature given according to (Wright & Okamura, 1977; Wright et al., 1972; Wright & Marsh, 2016). For the four cases we tested above, we observed virtually the same, consistent agreement between our simulation and the measured data. Hence, for simplicity's sake, we took $d = 1$ in our simulations, whence our values for τ, ω_ϕ^2, and H in Table 1 follow.

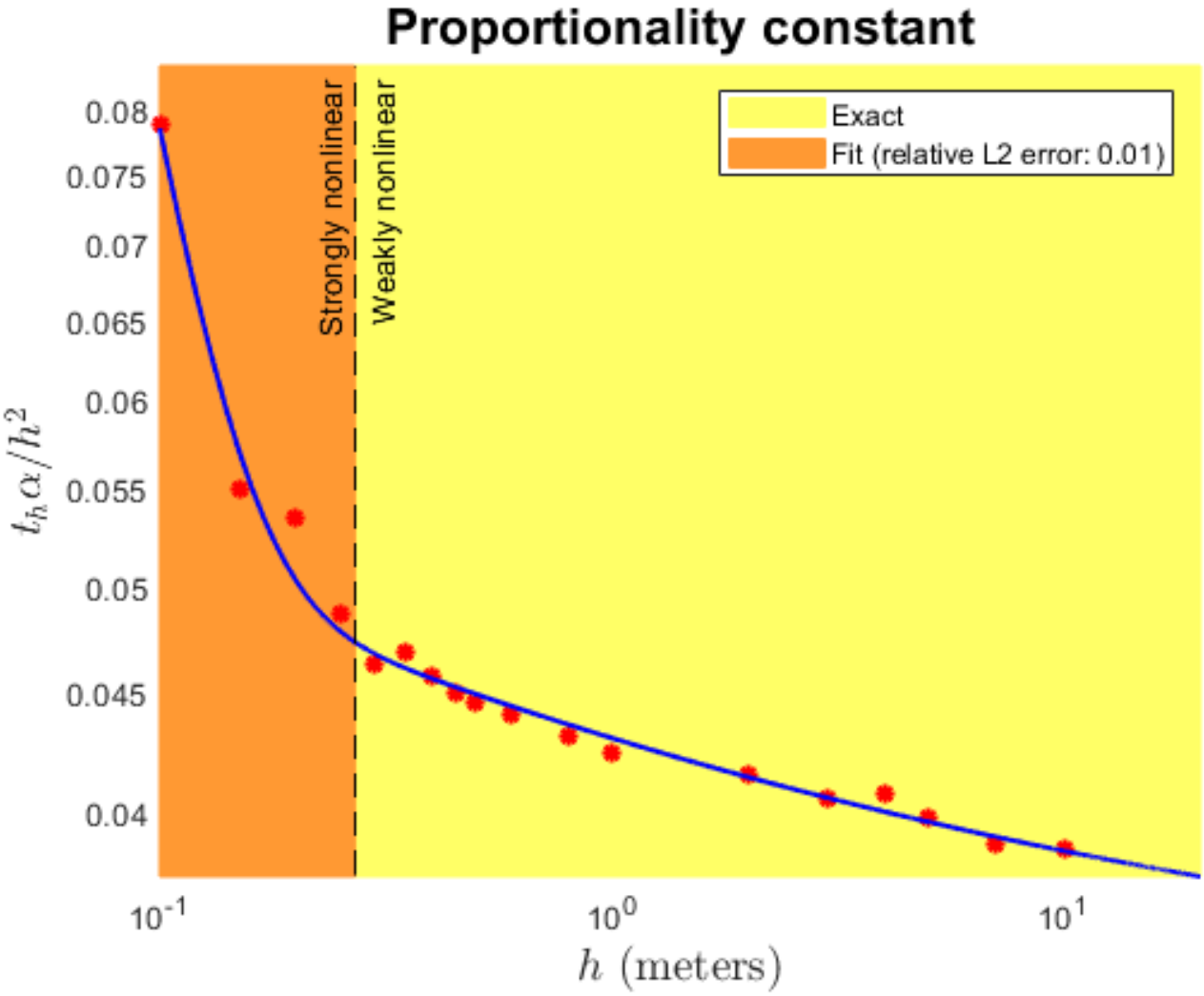

Figure S2. The caption was too large to be included here, and hence is contained in the text.

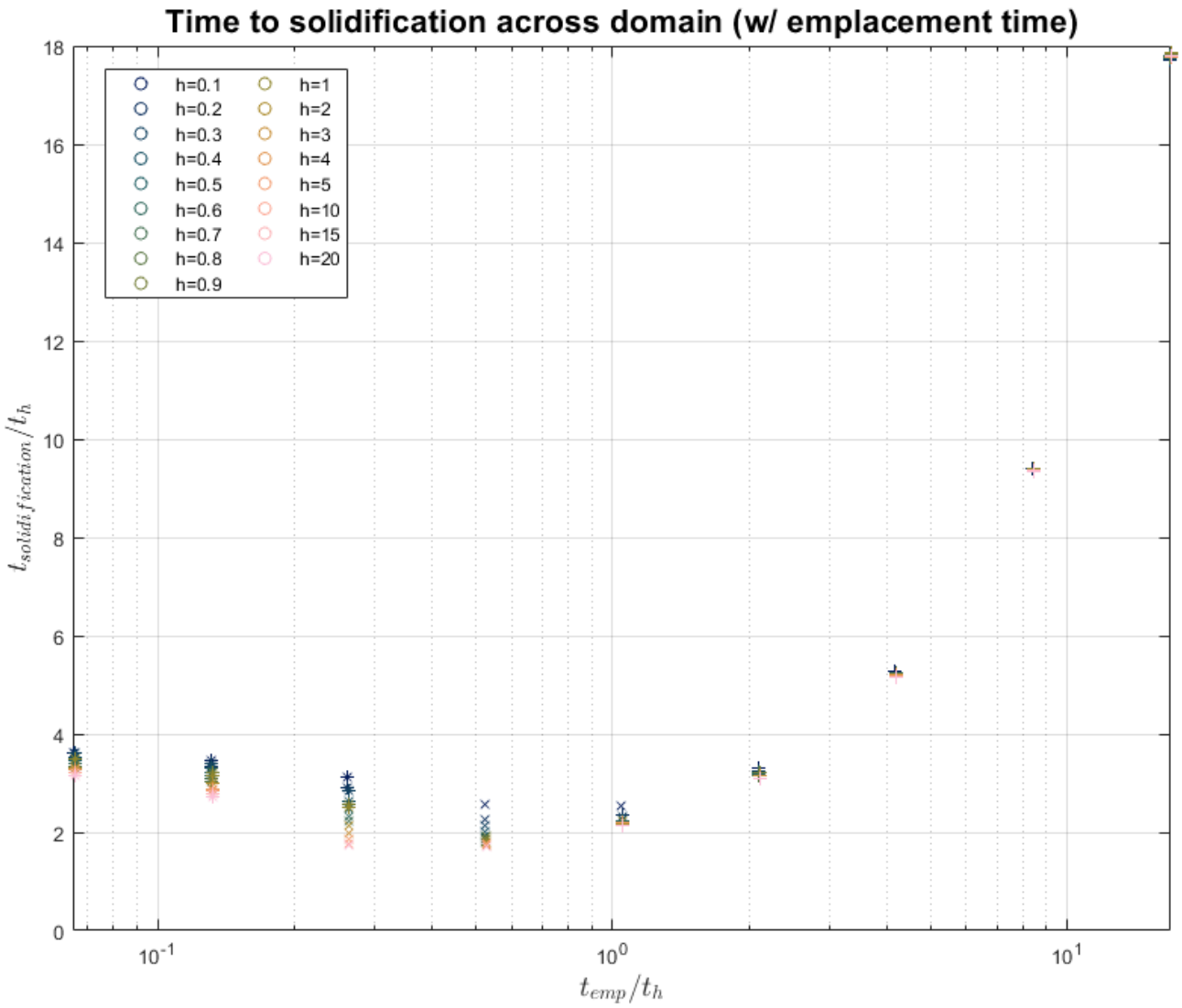

Figure S3. (Compare with Figure S4.) The dimensionless log-log plot above shows the solidification time including the time between emplacement, $t_{\text{solidification}}$, as a function of the emplacement time interval, t_{emp}, with both axes scaled by t_h. Note in particular that the graph at any lobe size has a minimum near or slightly below $t_{\text{emp}} = t_h$. This minimum reflects some optimal balance between the emplacement time and the thermal/phase interaction between the two lobes which minimizes the solidification time across the domain. This optimal balance lies within the in parallel region.

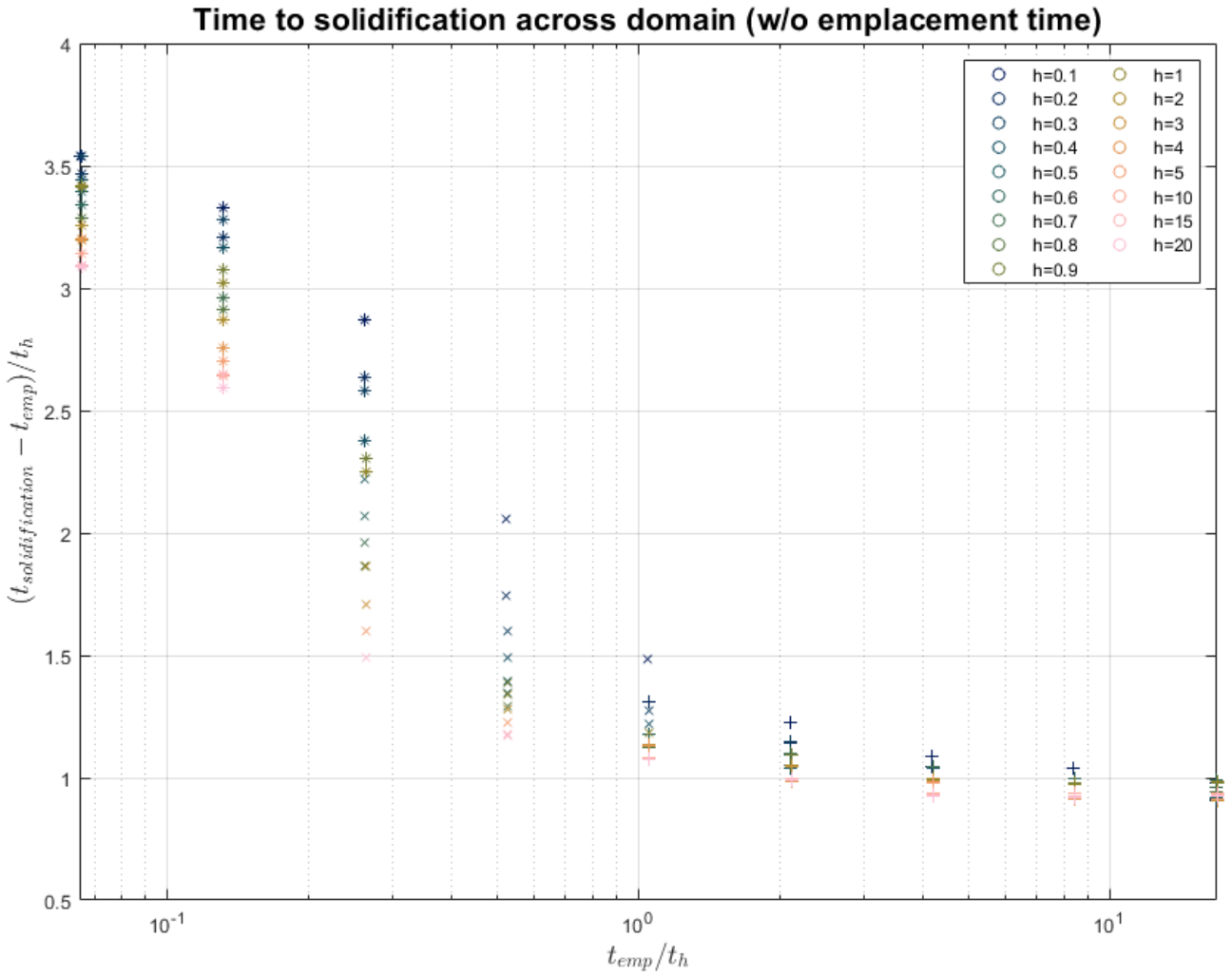

Figure S4. The above plot highlights an alternate interpretation of the solidification time in which we neglect the time between emplacements. On either plot, we note that as $t_{\text{emp}} \to 0$, $t_{\text{solidification}} \to 4t_h$. This reflects how, since $t_h \sim h^2$, $t_{2h} \sim (2h)^2 = 4h^2$. Meanwhile, in comparison to Figure S3, this plot better demonstrates how as $t_{\text{emp}} \to \infty$, $t_{\text{solidification}} \to t_h + t_{\text{emp}}$.

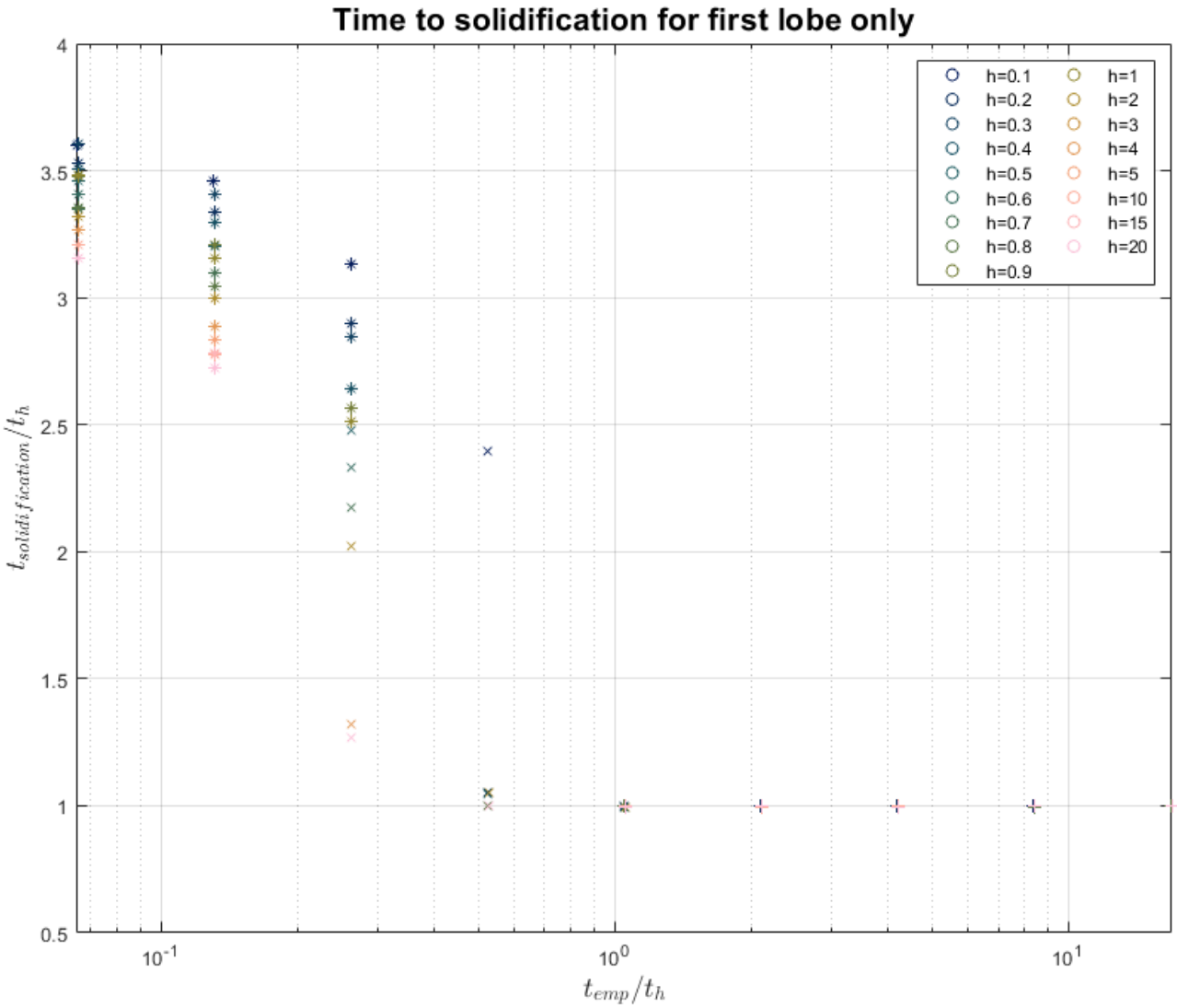

Figure S5. The above plot only considers the time for the first lobe to solidify vs. t_{emp}/t_h, thereby highlighting the thermal influence of the upper lobe upon how the lower lobe solidifies relative to t_h. As expected, $t_{\text{solidification}} \to t_h$ when $t_{\text{emp}} \to \infty$. Physically, we can interpret this result as follows: If the lower lobe has fully solidified before the upper lobe is emplaced, then the upper lobe will have no influence on the solidification of the lower lobe.

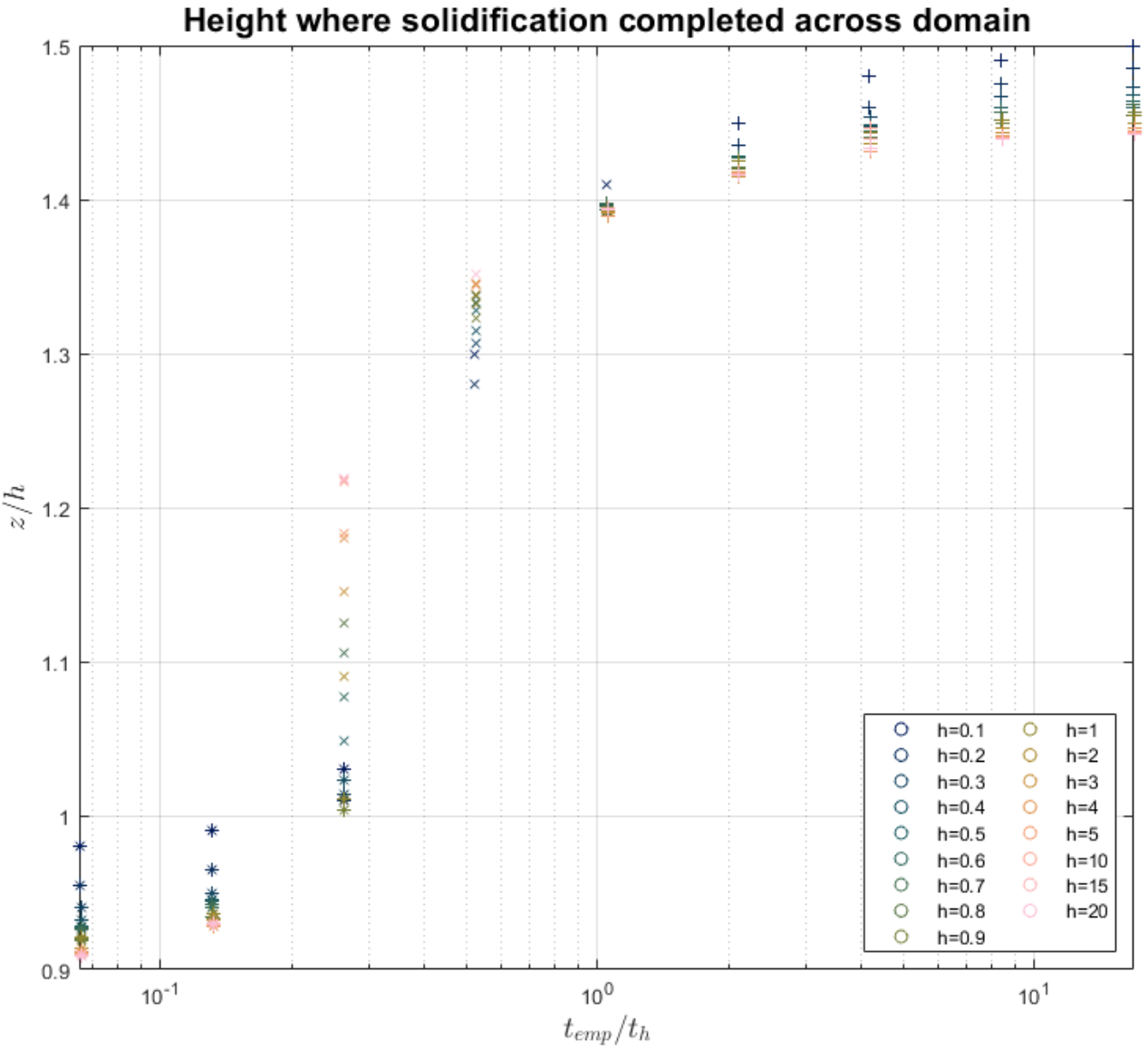

Figure S6. This plot indicates the height, scaled to the lobe size, at which solidification completed across the entire two-lobe system vs. t_{emp}/t_h. This variable is significant because horizontal fractures often form wherever solidification completes in a lava lobe, i.e., where two solidifying fronts meet. Note in particular that the smaller lobe sizes appear to have greater solidification heights in the merged and in sequence regions, while the opposite behavior is observed for the in parallel region. The quantitative differences in behavior across different lobe sizes appears to be greatest for the in parallel region, which we also see in Figure S7.

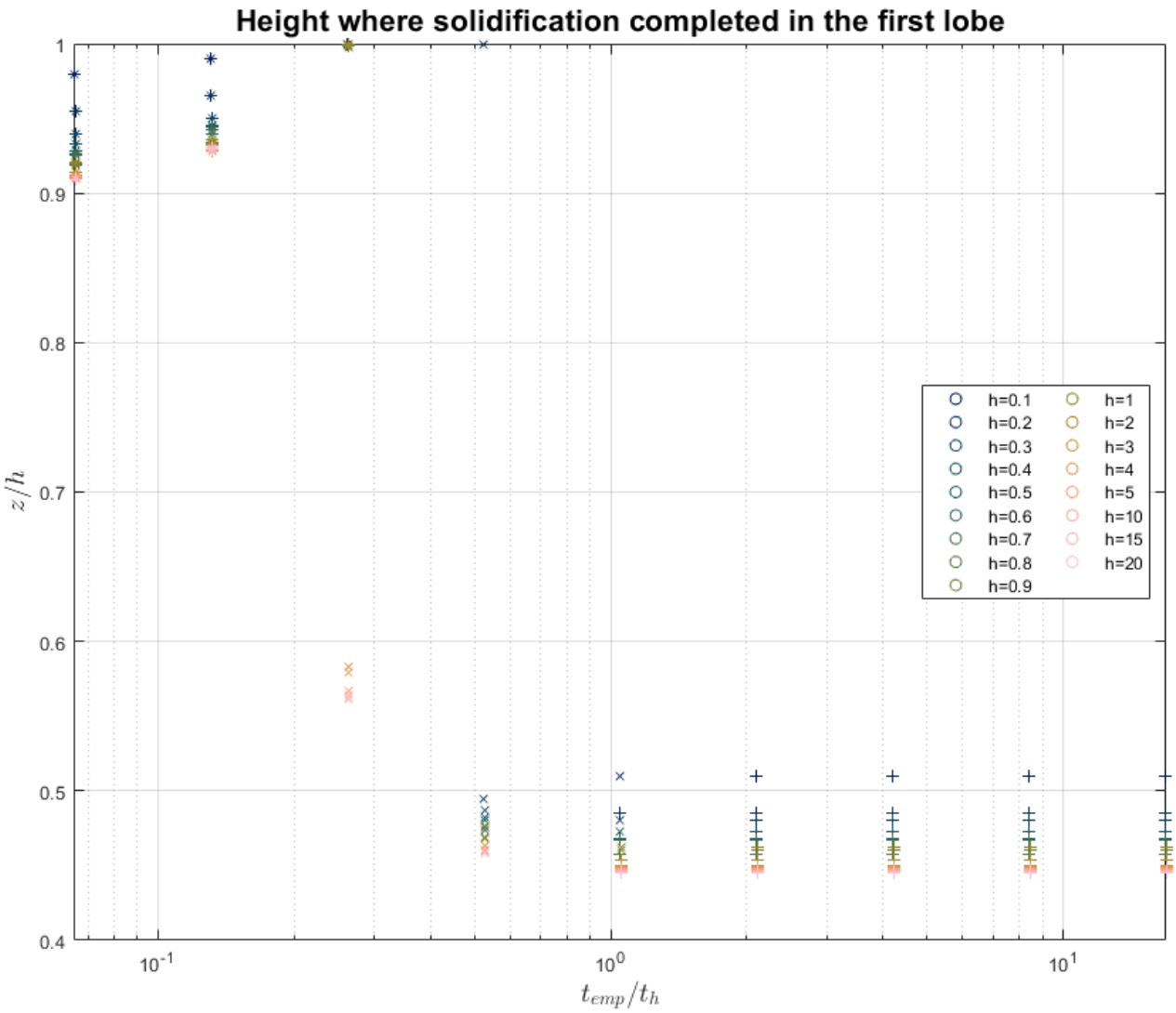

Figure S7. This plot is the same as Figure S6, except that this plot measures solidification in the first lobe only, i.e., where the first lobe solidified. Note that for a given height, the graph appears to increase during the fused region, decrease sharply during the in parallel region, and then finally level out during the in sequence region. The trend in the in parallel region appears to be sharper the smaller the lobe size is, which indicates how the thermal influence of the upper lobe on the lower lobe increases as the lobe size decreases, assuming that the lobes do not just merge entirely. As with Figure S6, the greatest disparity in dynamics across different lobe sizes seems to be greatest for the in parallel region.